Nanoscale Path Planning and Motion Control

Huzefa Shakir, *Student Member, IEEE*, and Won-jong Kim, *Senior Member, IEEE*

***Abstract*—This paper addresses nanoscale path planning and motion control, which is essential in key nanomanufacturing applications such as microstereolithography (μSTL), dip-pen-nanolithography (DPN), and scanning applications for imaging and manipulation of nanoscale surface phenomena, with the magnetic-levitation (maglev) technology. We identified motion trajectories commonly used in industrial applications along with the challenges in optimal path planning to meet the nanoscale motion-control objectives and achieve precise positioning and maximum throughput simultaneously. Key control parameters in path planning are determined, and control design methodologies including a well-damped lead-lag controller and an optimal linear quadratic regulator are proposed to satisfy the positioning requirements. The proposed methodologies, individually and collectively, were implemented, and experimental results are presented in this paper to illustrate their effectiveness in planning optimal trajectories. The damped lead-lag controller exhibited the command overshoot of as small as 0.37%, and the multivariable LQ controller reduced the dynamic coupling between the axes by 97.1% as compared with the decoupled single-input-single-output (SISO) lead-lag controllers. The position resolution of 5 nm was achieved in *x* and *y* with the errors in command tracking as small as 4.5 nm. The maglev stage demonstrated excellent performances for the chosen nanomanufacturing applications in terms of position resolution and accuracy, and speed.**

***Index Terms*—Nanomanipulation, nanomanufacturing, maglev system, precision positioning, nanoscale path planning, multivariable optimal control.**

I. Introduction

Manufacturing at nanoscale is one of the major research-and-development focus areas in the application of the nanotechnology and has significant economic and societal impacts [1]–[2]. The development of the scanning tunneling microscope (STM) and the atomic force microscope (ATM) initiated a variety of atomic-level profiling and characterizing instruments. These scanning probe microscopes (SPMs) were originally intended for molecular and atomic-level topographic imaging. In the last decade, however, the STM/AFM became one of the key instruments in nanoscale manipulation [3]. However, the fundamental limitation of the manipulation methodology with an STM/AFM is that these manipulators have only limited 2-dimensional (2D) motion capability with small (several micrometers) vertical motion without rotational motion capabilities. Moreover, PZT (lead zirconate titanate) ceramics frequently used in the piezoelectric actuators of an STM/AFM has several major downsides, including thermal drift, hysteresis, limited linear range, and high operation voltage. Because of these drawbacks, these SPM-based manipulators alone cannot be used as nanomanufacturing tools. Thus, novel actuation and sensing mechanisms are needed to meet the demanding specifications in nanoscale manufacturing.

The maglev technology has been demonstrated successfully for nanopositioning applications. Several research groups developed precision positioning devices using this technology. Kim, Shan *et al*., and Holmes *et al*. have done some pioneering work in high-precision magnetic levitation [4]–[6]. Verma *et al*. describes in detail the maglev stage we use as a test bed in this paper [7]. The main benefit of magnetic levitation over other prevailing technologies is its non-contact nature while in operation, i.e. the forces are applied to the moving part without any mechanical contact. Thus there is no friction, hysteresis, or backlash. This maglev technology is suitable for clean-room or vacuum environments since it does not require any lubricants or generate wear particles. Furthermore, without complex mechanical elements, the fabrication cost can be substantially reduced.

Among the various potential applications of the maglev nanopositioning device is the manufacture of small objects. One of the most important tasks herein is nanomanipulation, which essentially enables to position, orient, and fabricate at nanoscale precision. The maglev stage in conjunction with relevant manufacturing technologies, which can provide with fabrication and assembly at micro-level, will be able to produce micro-sized objects. In such applications this maglev stage will be used as the positioning device, and the fabrication/scanning of parts can be done with a fixed tool.

One of such techniques is μSTL. Classical STL processes use a laser beam deflected by a pair of low-inertia-galvanometric mirrors and focused by a dynamic lens to solidify photopolymer [8]. This methodology works well for objects on the order of a few hundred micrometers. However, beam defocusing becomes problematic for smaller objects. An alternate approach is to keep the laser beam fixed and use a high-precision positioning stage to

Manuscript received February 9, 2005. This work was supported by the National Science Foundation under Grant No. CMS-0116642.

H. Shakir is with the Department of Mechanical Engineering, Texas A&M University, College Station, TX 77840 USA (phone: 979-845-2224; fax: 979-845-3989; e-mail: huzefa@tamu.edu).

W.-J. Kim is with the Department of Mechanical Engineering, Texas A&M University, College Station, TX 77843-3123 USA (phone: 979-845-3645; fax: 979-862-3989; e-mail: wjkim@mengr.tamu.edu).

generate *x*-*y* motions for scanning [9]. Beluze *et al.* and Zhang *et al.* have used this kind of *x*-*y* stages for μSTL [10]–[11]. Ikuta *et al.* showed the capability of such stages for the mass integrated harden polymer stereolithography process [12]. However, in all these processes, the minimum achievable part size is limited by the position resolution of the stage being used. In the work presented herein, we have demonstrated that this limitation in positioning can be easily overcome with our maglev stage.

Since only a single maglev moving part, namely the platen, generates all the motions, its dynamics is coupled in 6 degrees of freedom (DOFs). Thus a linear multivariable quadratic control is a natural choice to regulate the position of the platen. We designed and implemented a multivariable linear quadratic regulator (LQR) for the lateral modes (*x*, *y* and the angle about the *z*-axis) of the maglev stage [13]. There are many research results on macroscopic time-optimal control especially in path planning in robotics [14]–[16]. However, no significant literature is available for manufacturing applications at nanoscale. Although we have used well-established classical and modern control techniques to design the controllers, our methodologies enable path planning and motion control at nanoscale. Other application-specific path optimization and motion control techniques need to be employed to meet the performance objectives at nanoscale.

This paper is organized as follows. Section II gives a brief description of the maglev stage. The concept of nanoscale path planning is introduced in Section III with basic trajectories to emulate real-life applications and to deal with challenges in path planning and motion control at nanoscale. Section IV describes the design and implementation of a multivariable LQR motion controller for the lateral modes of the nanopositioning maglev stage to achieve a critically damped trajectory without compromising the rise time and the settling time. Experimental results for general trajectories relevant to nanomanufacturing using the proposed methodologies are presented and discussed in Section V.

II. Maglev Stage Overview

A photograph of the mechanical assembly of the maglev stage is shown in Fig. 1. A single moving part, namely the platen, consists of a triangular aluminum part pocket-milled to reduce the mass while maintaining the structural stiffness for high natural frequency. The total mass of moving part is 0.2126 kg, and the total power consumption by all the actuators is only a fraction of a watt. There are six sets of magnets for six single-axis actuators. The coils for all six actuators are mounted on a stationary aluminum base plate via coil holders. There are three plane mirrors attached to the sides of the platen, and horizontal motion sensing at subnanometer resolution is achieved with HeNe laser interferometers. For vertical motion sensing, we have three

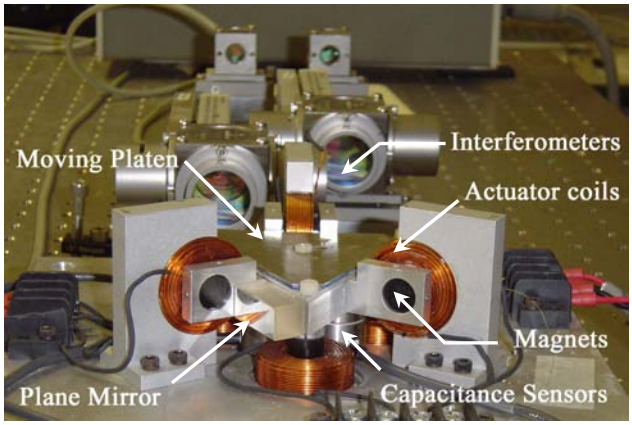

Fig. 1. Photograph of the maglev stage.

capacitance gauges mounted on the base plate right below the platen. The six-axis motions are generated by the application of six independent force components. A combination of horizontal forces makes the platen move in *x*, *y*, or φ and a combination of vertical forces makes it move in *z*, θ, or ψ. A detailed description of the mechanical and instrumentation structure can be found in [7].

III. Nanoscale Path Planning

Fig. 2 shows the actual path followed by the platen that can be employed in a μSTL application with the controller given in [7]. The actual path significantly overshot the desired trajectory. This is because the controller was not optimized for speed, and the platen did not begin the corner turns until the actual path overshot the command. Furthermore, since the controllers were simple lead-lag compensators, there was no direct control over the velocity. Coupling between the *x*- and *y*-axes was also significant as seen in Fig. 2 since the controllers were SISO ones. In the following sections, an attempt is made to reduce these shortcomings for better trajectory-tracking.

A. Overshoot Reduction

There are various ways through which the overshoot may be reduced.

1) Using smaller yet uniform position-command steps: Since the plant is assumed to be linear, the overshoot is proportional to the step size. Hence the overall overshoot can be significantly reduced by using successive smaller position-command steps instead of a single large one. Fig. 2 shows the path followed by the stage using smaller uniform steps of 5 μm against the larger 20-μm and 25-μm steps used previously to cover the same distance. The overall percentage overshoot was reduced to 6.58% from 39.35% in *x* and to 5.05% from 31.99% in *y*.

2) Using decreasing position-command steps: An alternate method is to use decreasing step-command sizes. It, in effect, slows down the platen as it approaches the corners. Fig. 2 shows the path followed by the stage using the step-sizes decreasing in a geometric progression (12.5,

6.25, 3.125, 1.5625, and 1.5625 μm). The overall percentage overshoot was reduced prominently to 2.32% from 39.35% in *x* and 2.12% from 31.99% in *y*. For the above two trajectory-planning experiments, we used a controller with a 47.5-Hz crossover frequency and 51° phase margin (PM).

3) Using a damped controller: The above two methods, however, depend on the nature of the trajectory and give little flexibility. Furthermore, applications like scanning demands a much better transient response and any overshoot is unacceptable. A better way to tackle the problem is to design a well-damped controller that gives a lesser overshoot. We designed another controller with a larger crossover frequency of 85.8 Hz and 73° PM to meet the conflicting requirements of lesser overshoot and faster dynamic responses simultaneously.

B. Velocity Control

Another parameter to be controlled in trajectory-tracking is the velocity. We need the platen to slow down as it approaches the corners (as shown in Fig. 2) for sharper maneuver. Similarly, in the trajectories which require continuous directional changes, it is crucial to have a precise control over the velocity in addition to the position. One way to control the velocity is, again, through controlling the command step size. The implementation of the controller in the form of difference equations requires steps at fixed time intervals (0.2 ms for our case at the sampling rate of 5 kHz). Varying the step size for the fixed time intervals is thus equivalent to varying the speed of the platen.

Fig. 3 shows the effect of varying the speed of the platen. It shows the same trajectory followed by the platen as shown in Fig. 2 but with the spatial scale reduction by a factor of 100. As the speed of the platen was reduced from 50 μm/s to 5 μm/s, the position accuracy of the platen was dramatically improved. The position-noise level varied from the best of 4.5 nm to the worst of 10.5 nm (peak-to-peak). The maximum deviation from the trajectory was found to be 8.5 nm.

C. Nanoscale Trajectory Tracking

The above two methodologies combined together can drastically improve trajectory-tracking. Fig. 4 shows the same trajectory followed using these path-planning methodologies as the one originally shown in Fig. 2. The path was traversed with a constant velocity of 50 μm/s. A comparison between the two trajectories shows that the percentage overshoot was reduced to 0.45% from 39.35% in *x* and to 0.37% from 31.99% in *y*. The maximum steady-state error was reduced to 18.2 nm from 20.6 nm. However, the total time taken to trace the entire trajectory increased from 0.17 s to 1.7 s. This time increase, however, is acceptable for an application like μSTL that works at a much slower rate [8].

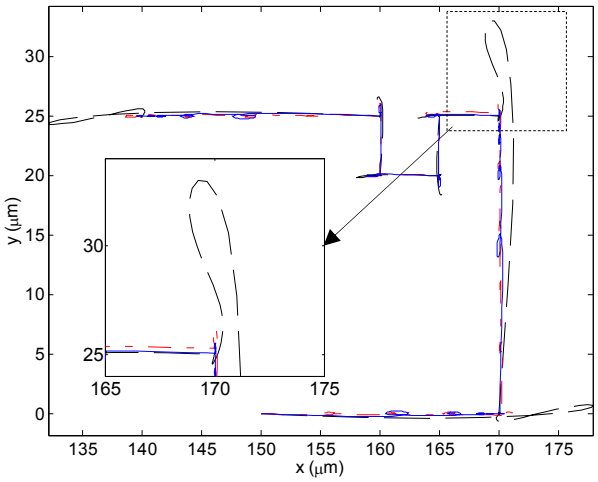

Fig. 2. Path traversed by the platen without using path-planning methodologies (dashed), with smaller uniform steps of 5 μm (dash-dotted), and with decreasing step commands (solid).

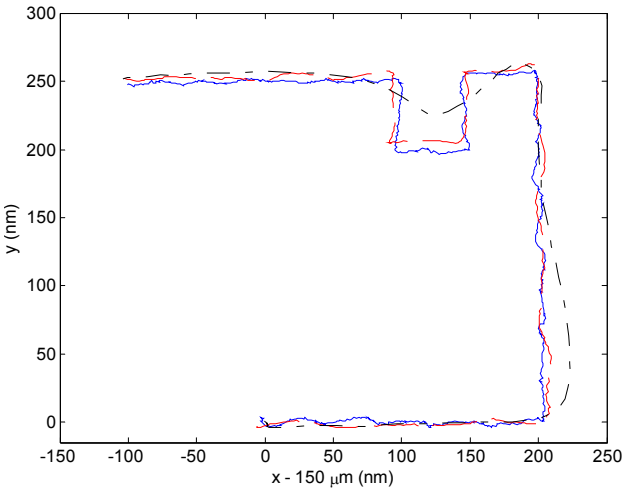

Fig. 3. Path traversed by the platen at nanoscale. Dash-dotted line: 50 μm/s, dashed line: 25 μm/s, and solid line: 5 μm/s.

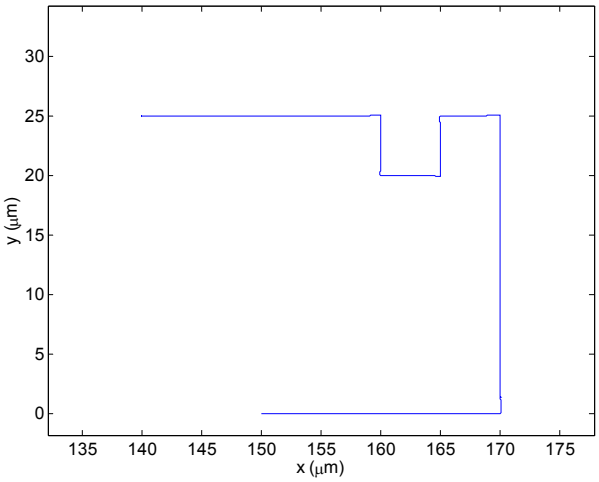

Fig. 4. Path traversed by the platen using the path-planning methodologies.

IV. Multivariable LQ Control

Since there is only one moving part that generates all the 6-DOF motions, its dynamics is coupled. The path-planning methodologies discussed above do not address this dynamic coupling since we designed the SISO controllers assuming that the dynamics of the platen is decoupled in all 6 axes. Furthermore, direct velocity feedback was not used by the controllers. This gives rise to the need of designing an advanced controller. A multivariable LQ control scheme has been developed and implemented for this purpose.

A. Plant Modeling and Linearization

In order to develop high-performance controllers, precise dynamic modeling is required. To start with, we decoupled the plant into two modes, vertical and lateral, against all the six decoupled axes used previously. We designed an LQR for the lateral modes (x, y and angle about the z-axis, φ) and kept the decoupled SISO lead-lag controllers for the vertical modes (z, angle about the x-axis, ψ and angle about the y-axis, θ). The reason for this choice is that we do not need to differentiate the position data or build a state estimator for velocity feedback for the lateral control since full-state feedback is provided by the laser-interferometer electronics.

To apply the multivariable control, a state-space model of the platen dynamics was derived. The full equations of motion are nonlinear because of the nonlinear current-force characteristics of the actuators as well as the dependence of the platen motion on the trigonometric functions of the angles of rotation with respect to the inertial frame. A detailed analysis and linearization was discussed in [13]. Here we present the final state-space equations for the lateral mode directly, given as follows.

$$\begin{bmatrix} \dot{\tilde{x}} \\ \dot{\tilde{y}} \\ \dot{\tilde{\phi}} \\ \dot{\tilde{u}} \\ \dot{\tilde{v}} \\ \dot{\tilde{r}} \end{bmatrix} = \begin{bmatrix} 0 & 0 & 0 & 1 & 0 & 0 \\ 0 & 0 & 0 & 0 & 1 & 0 \\ 0 & 0 & 0 & 0 & 0 & 1 \\ 0 & 0 & 0 & 0 & 0 & 0 \\ 0 & 0 & 0 & 0 & 0 & 0 \\ 0 & 0 & 0 & 0 & 0 & 0 \end{bmatrix} \begin{bmatrix} \tilde{x} \\ \tilde{y} \\ \tilde{\phi} \\ \tilde{u} \\ \tilde{v} \\ \tilde{r} \end{bmatrix} + \begin{bmatrix} 0 & 0 & 0 \\ 0 & 0 & 0 \\ 0 & 0 & 0 \\ 7.8921 & -3.9460 & -3.9460 \\ 0 & 6.8347 & -6.8347 \\ 287.2842 & 292.3645 & 297.425 \end{bmatrix} \begin{bmatrix} \tilde{i}_4 \\ \tilde{i}_5 \\ \tilde{i}_6 \end{bmatrix}, \tag{1}$$

where i_4, i_5, and i_6 are the currents in the horizontal actuators. The tilde (~) above the state variables indicates that they are small-signal variables about an operating point.

B. Linear Quadratic Regulation for Lateral Control

With the pure-mass model without friction we are using, the plant transfer function should have a double pole at the origin of the s-plane theoretically. However in practice, the plant poles may not be located precisely at the origin, and consequently, there can be a non-zero steady-state error. To deal with this problem, we augmented the plant model with integrators to eliminate this steady-state error. In our case, we are interested in position-command tracking, so we use three integrators, each for x, y and φ.

Consider the plant represented by the following differential equations in state-space form

$$\begin{aligned} \dot{\boldsymbol{x}}_p &= A_p \boldsymbol{x}_p + B_p \boldsymbol{u}_p \\ \boldsymbol{y}_p &= C_p \boldsymbol{x}_p \end{aligned}. \tag{2}$$

Defining the new state vector $\boldsymbol{\xi}_p$ as

$$\dot{\boldsymbol{\xi}}_p = \boldsymbol{y}_p = C_p \boldsymbol{x}_p, \tag{3}$$

we get the augmented system dynamics as

$$\begin{aligned} \dot{\boldsymbol{x}} &= \begin{bmatrix} \dot{\boldsymbol{x}}_p \\ \dot{\boldsymbol{\xi}}_p \end{bmatrix} = \begin{bmatrix} A_p & 0 \\ C_p & 0 \end{bmatrix} \begin{bmatrix} \boldsymbol{x}_p \\ \boldsymbol{\xi}_p \end{bmatrix} + \begin{bmatrix} B_p \\ 0 \end{bmatrix} \boldsymbol{u}_p \\ \boldsymbol{y}_p &= \begin{bmatrix} C_p & 0 \end{bmatrix} \begin{bmatrix} \boldsymbol{x}_p \\ \boldsymbol{\xi}_p \end{bmatrix} \end{aligned}. \tag{4}$$

Define the performance index as

$$\boldsymbol{J}(\boldsymbol{x}(\cdot), \boldsymbol{u}_p(\cdot), t_0) = \int_{t_0}^{\infty} \left(\boldsymbol{u}_p{}^T(t) R \boldsymbol{u}_p(t) + \boldsymbol{x}^T(t) Q \boldsymbol{x}(t) \right) dt \,. \tag{5}$$

This time-invariant infinite-time regulator problem is a minimization problem to find an optimal control $\boldsymbol{u}_p{}^*$ to minimize $\boldsymbol{J}$. The solution of this problem is well-known and can be found in texts on optimal control such as [17].

Design and test results of the LQ controller were reported in [13]. The multivariable LQ control significantly reduced the dynamic coupling by 91.6% in y and 97.1% in φ [13]. This reduction in the dynamic coupling was calculated by the percentage change in the maximum perturbation from the commanded position in y and φ when a step-command is given in x.

V. Test Results for Key Nanomanufacturing Applications

In this section, we apply the proposed methodologies to generate trajectories relevant to key nanomanufacturing applications such as DPN, μSTL, and scanning, and the effectiveness of the path-planning techniques is demonstrated.

A. Dip-Pen-Nanolithography

One of the practical applications which require extensive nanoscale path planning is DPN. Nanoink, Inc. has been a major player in this area. Their scanning stage is motor-driven, and hence requires intensive maintenance and suffers losses due to friction from its contact-type mechanisms [18]. Furthermore, the apparatus uses 7 motors for translation and zoom against the single-moving-part approach of the maglev stage we designed. Thus, our maglev system is much simpler and provides competitive advantages in similar applications.

Fig. 5(a) shows such a trajectory traversed by the maglev platen. This may be considered as a main reservoir of 10-μm diameter with four micro-fluidic channels of 314-nm width and "nanowells" of 1-μm diameter to be used in

DPN for ink coating. The entire trajectory was traversed at variable speeds, 10 µm/s for the channels, 14.14 µm/s for the nanowell, and 15.55 µm/s for the reservoir. The total time taken to complete this trajectory was 6.8 s. The errors in x and y in the command-tracking are shown in Fig. 5(b) and (c).

B. *Microstereolithography*

With its inception in the early 1990's, remarkable research progresses have been made in microelectromechanical systems (MEMS). Many MEMS device concepts were proposed, and their feasibility was demonstrated for applications in various fields of microfluids, aerospace, biomedical, chemical analysis, wireless communications, data storage, display, optics, etc. [9]. Manufacturing processes, such as µSTL, micromachining, micromolding, and soft-lithography played a crucial role in the miniaturization of MEMS devices. However, the minimum achievable component size remains the limiting factor with the critical issues such as resolution and precision positioning. Magnetic levitation became an enabling technology for these applications with position resolution as good as 5 nm [7].

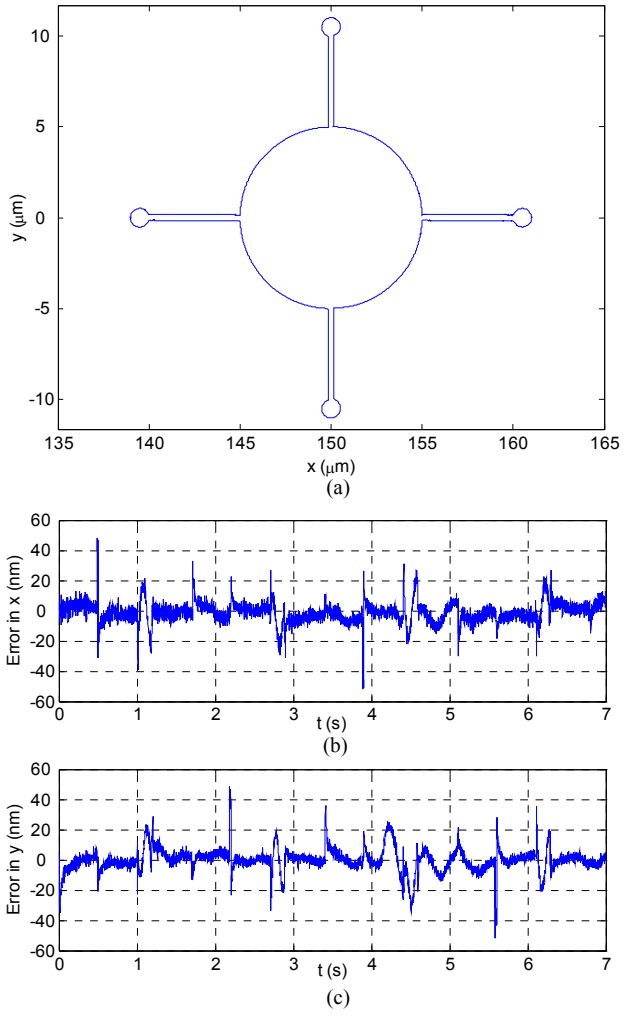

Fig. 5. (a) Path traversed by the maglev platen to track a four-channel nanowell. Errors in the trajectory followed (b) in x and (c) in y.

Fig. 6 shows a microscale screw for medical tissues traced by our maglev stage with the lateral resolution of 5 nm and vertical resolution of 100 nm. The inner radius, the outer radius, the pitch, and the length of the threads are 10 µm, 13.75 µm, 6 µm, and 60 µm, respectively. The state of the art is the one fabricated by the Central Microstructure Facility with a lateral and vertical position resolution of 10 µm, inner radius of 1200 µm, thread length of 900 µm, and pitch of 150 µm, approximately [19].

C. *Scanning Applications*

Among commonly used scanning devices are (1) piezo-based scanners to position a probe on a sample surface during imaging of nanoscale surface phenomena with SPMs and (2) MEMS-based scanners to position optical micro-mirrors in wearable computers [14]. An alternative is to keep the probe fixed and move the stage in the x-y plane to scan the surface.

A typical scanning operation consists of two sections: (1) the active-scan or output-tracking section where a desired output trajectory is pre-specified and must be tracked precisely and (2) the retrace or output-transition section where trajectory-tracking is not critical. Instead, the output is to be returned to a predefined value so that the active scan can be repeated [14]. These active-scan and retrace sections are repeated in time in a scanning operation. Fig. 7 shows a simple scan trajectory traced by the maglev stage to demonstrate its precision scanning capability in the active-scan section as well as fast return motion in the retrace section. Paths 1-2, 3-4, and 5-6 are active-scan trajectories, and paths 2-3, 4-5, and 6-1 are fast retrace trajectories. The error in the active-scan section is well within 40 nm peak-to-peak in x and 60 nm peak-to-peak in y. The tracking speed and the return speed are 50 µm/s and 500 µm/s, respectively.

VI. Conclusions

With the recent development in nanomanipulation and nanomanufacturing, appropriate path-planning techniques are required as much as precision positioning itself. Although substantial research results are available on macroscopic trajectory planning and control, particularly in robotic applications, not much work has been reported yet in nanoscale path planning and motion control. In this paper, we investigated key problems we may face while actually putting in use nanomanipulation devices, more specifically, incorporating a maglev stage as a test bed in manufacturing or scanning applications at nanoscale.

The control parameters that influence the dynamic behavior of the positioning device were identified, and ways to control these parameters were proposed. Design and implementation of a well-damped SISO lead-lag

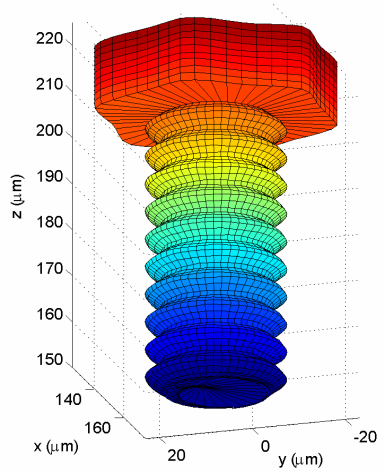

Fig. 6. 3D profile traced by the platen to manufacture a microscale screw for medical tissues with μSTL.

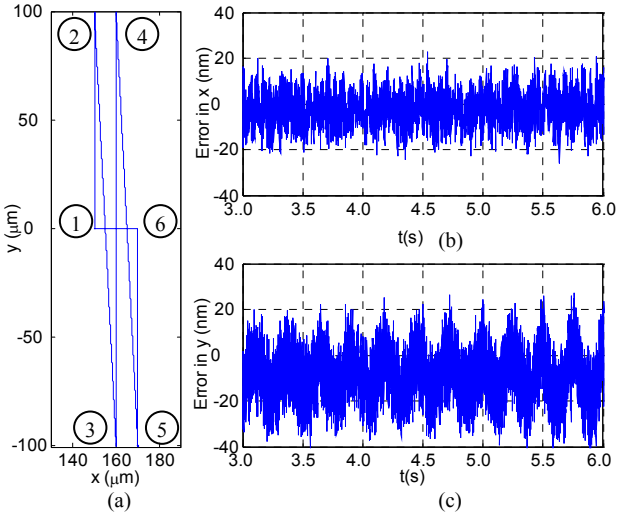

Fig. 7. (a) Active-scan and retrace sections scanned by the platen. (b) Error in *x* and (c) in *y*.

controller and a multivariable LQ controller was described, and their influence on the performance of the maglev stage was discussed. Increasing the damping and reducing the velocity decreased the overall percentage overshoot to 0.45% from 39.35% in *x* and to 0.37% from 31.99% in *y* while cornering, thereby improving the dynamic performance significantly. The use of multivariable control ensured 91.6% lesser coupling in *y* and 97.1%, in φ.

Test results for key nanomanufacturing applications such as μSTL, DPN, and scanning were presented. A position resolution of 5 nm in *x* and *y* was achieved, and the errors in command tracking were well within 40 nm peak-to-peak with the best performance of 4.5 nm. The minimum achievable component size is thus limited only by manufacturing techniques and not by the positioning technology. The experimental results demonstrated that the maglev stage performed well for these nanomanufacturing applications in terms of position resolution, accuracy, speed, and versatility.

ACKNOWLEDGMENTS

The authors thank Jie Gu and Shobhit Verma for their contributions in design, assembly, and software development for the maglev test bed.

REFERENCES

[1] National Nanotechnology Initiative [Online]. Available: http://www.nano.gov/html/research/nnigc.html.

[2] H. Doumanidis, "The nanomanufacturing programme at the National Science Foundation," *Nanotechnology*, vol. 13, no. 3, pp. 248–252, Apr. 2002.

[3] L. T. Hansen, A. Kuhle, A. H. Sorensen, J. Bohr, and P. E. Lindelof, "A technique for positioning nanoparticles using an atomic force microscope," *Nanotechnology*, vol. 9, no. 4, pp. 337–342, Dec. 1998.

[4] W.-J. Kim, "High-precision planar magnetic levitation," Ph.D. Dissertation, Dept. of Elect. Eng., Massachusetts Institute of Technology, Cambridge, MA, June 1997.

[5] X. Shan, S.-K. Kuo, J. Zhang, and C.-H. Menq, "Ultra precision motion control of a multiple degrees of freedom magnetic suspension stage," *IEEE/ASME Tr. on Mechatronics*, vol. 7, no. 1, pp. 67–78, Mar. 2002.

[6] M. Holmes, R. Hocken, and D. L. Trumper, "The long-range scanning stage: a novel platform for scanned-probe microscopy," *Precision Engineering*, vol. 24, no. 3, pp. 191–209, July 2000.

[7] S. Verma, W.-J. Kim, and J. Gu, "Six-axis nanopositioning device with precision magnetic levitation technology," *IEEE/ASME Tr. on Mechatronics*, vol. 9, no. 2, pp. 384–391, June 2004.

[8] P. F. Jacobs, *Stereolithography and other RP&M Technologies*. ASME Press, New York, 1996.

[9] V. K. Vardan, X. Jiang, and V. V. Vardan, *Microstereolithography and other Fabrication Techniques for 3D MEMS*. John Wiley and Sons, 2001, pp. 111–127.

[10] L. Beluze, A. Bertsch, and P. Renaud, "Microstereolithography: A new process to build complex 3D objects," in *Proc. SPIE*, vol. 3680, pp. 808–817, Apr. 1999.

[11] X. Zhang, X. N. Jiang, and C. Sun, "Microstereolithography of polymeric and ceramic microstructures," *Sensors and Actuators A (Physical)*, vol. A77, no. 2, pp. 149–156, Mar. 1999.

[12] K. Ikuta, S. Maruo, and S. Kojima, "New microstereolithography for freely movable 3D microstructure–super IH process with submicron resolution," in *Proc. IEEE MEMS*, pp. 290–295, Jan. 1998.

[13] H. Shakir, W.-J. Kim, and S. Verma, "System identification and optimal control of a 6-DOF magnetic levitation stage with nanopositioning capabilities," in *Proc. of ASME IMECE 2004*, paper no. 60507, Nov. 2004.

[14] H. Perez, Q. Zou, and S. Devasia, "Design and control of optimal scan trajectories: scanning tunneling microscope example," *Journal of Dynamical Systems, Measurement and Control*, vol. 126, no. 1, pp 187–197, Mar. 2004.

[15] H. Chen, N. Xi, and Y. Chen, "Multi-objective optimal robot path planning in manufacturing," in *Proc. Intelligent Robots and Systems*, vol. 2, pp. 1167–1172, Oct. 2003.

[16] W.-J. Kim and D. L. Trumper, "Active multivariable optimal control of planar magnetic levitator," in *Proc. IEEE International Conference on Control Applications*, pp. 97–102, Oct. 1997.

[17] S. Stogestad and I. Postlewaite, *Multivariable Feedback Control*. John Wiley and Sons, 2003.

[18] NSCRIPTOR™ DPNWriter™ Hardware DataSheet. Nanoink inc. [Online]. Available: http://www.nanoink.net/3502_hardware.html.

[19] R. Lawes, (2002, Dec. 10). Microfabrication cost models for micromachining methods. Central Microstructure Facility [Online]. Available: http://www.cmf.rl.ac.uk/latest/msl.html.